Disease outbreak thresholds emerge from interactions between movement behavior, landscape structure, and epidemiology

Lauren A. White[a,1], James D. Forester[b], and Meggan E. Craft[c]

[a]Department of Ecology, Evolution & Behavior, University of Minnesota, St. Paul, MN 55108; [b]Department of Fisheries, Wildlife and Conservation Biology, University of Minnesota, St. Paul, MN 55108; and [c]Veterinary Population Medicine Department, University of Minnesota, St. Paul, MN 55108

Edited by Nils Chr. Stenseth, University of Oslo, Oslo, Norway, and approved May 29, 2018 (received for review January 24, 2018)

Disease models have provided conflicting evidence as to whether spatial heterogeneity promotes or impedes pathogen persistence. Moreover, there has been limited theoretical investigation into how animal movement behavior interacts with the spatial organization of resources (e.g., clustered, random, uniform) across a landscape to affect infectious disease dynamics. Importantly, spatial heterogeneity of resources can sometimes lead to nonlinear or counterintuitive outcomes depending on the host and pathogen system. There is a clear need to develop a general theoretical framework that could be used to create testable predictions for specific host–pathogen systems. Here, we develop an individual-based model integrated with movement ecology approaches to investigate how host movement behaviors interact with landscape heterogeneity (in the form of various levels of resource abundance and clustering) to affect pathogen dynamics. For most of the parameter space, our results support the counterintuitive idea that fragmentation promotes pathogen persistence, but this finding was largely dependent on perceptual range of the host, conspecific density, and recovery rate. For simulations with high conspecific density, slower recovery rates, and larger perceptual ranges, more complex disease dynamics emerged, and the most fragmented landscapes were not necessarily the most conducive to outbreaks or pathogen persistence. These results point to the importance of interactions between landscape structure, individual movement behavior, and pathogen transmission for predicting and understanding disease dynamics.

spatial heterogeneity | landscape fragmentation | disease model | resource selection function | perceptual range

Spatial heterogeneity—differences occurring across a geographic landscape—may arise from intrinsic differences between locations (e.g., resource abundance, quality, connectivity) or can emerge from stochastic or dynamic processes within populations (e.g., demographics, conspecific density) (1). The majority of disease models that incorporate spatial heterogeneity have focused primarily on a few well-studied wildlife systems (e.g., rabies and bovine tuberculosis [bTB]) or have been conducted in a purely theoretical context (2). Theoretical and simulation studies have provided evidence both for and against spatial heterogeneity promoting pathogen persistence (3–5), and the relative importance of local and long-distance processes is often unknown, except for in some well-studied diseases like rabies (2). Importantly, spatial heterogeneity may lead to nonlinear or counterintuitive outcomes depending on the host and pathogen system (4, 5).

Foraging, migration, and dispersal play an important role in creating spatial heterogeneity (6). Host movement and dispersal patterns can vary considerably (7), and infection with parasites can further alter those patterns (8). Both perceptual range (how far an individual can perceive habitat to be able to make movement choices) and movement capacity (the ability and efficiency with which an individual can move) can affect the realized connectivity of habitat patches in heterogeneous landscapes (9). While some models have explored the sensitivity of disease dynamics to dispersal and migration rates (2), few studies compare the effects of different movement rules over a spatially explicit landscape on pathogen transmission (5, 10). Moreover, disease models with mechanistic representations of animal movement remain rare (11).

In the realm of movement ecology, resource selection functions (RSFs) models have fostered a better understanding of how organisms navigate their surroundings (2, 12). While several studies have utilized RSFs to estimate interspecies contact risk, RSFs are not commonly used to infer transmission events (2). Moreover, cues, such as conspecific density, can also be important drivers of individual movement decisions but are rarely utilized when modeling habitat selection (13). In addition, it is difficult to validate movement model predictions in the context of pathogen transmission, because overlapping movement and pathogen transmission datasets are still uncommon (12). Many existing spatial disease models that explicitly incorporate individual movement rely on random or correlated random walks (5, 11). While adequate for some species at specific temporal scales, these approaches do not necessarily capture an individual's response to its immediate surroundings or its memory that might favor revisitation or avoidance of previous sites (14, 15).

Overall, we lack a mechanistic understanding of how host movement and habitat preferences across heterogeneous landscapes affect pathogen dynamics. Here, we asked the following

Significance

Understanding how emerging infectious and zoonotic diseases spread through space and time is critical for predicting outbreaks and designing interventions; disease models are important tools for realizing these goals. Currently, humans are altering the environment in unprecedented ways through urbanization, habitat fragmentation, and climate change. However, the consequences of increasingly heterogeneous landscapes on pathogen transmission and persistence remain unclear. By synthesizing mathematical modeling and movement ecology approaches, we examined how wildlife movement patterns interact with broad-scale landscape structure to affect population-level disease dynamics. We found that habitat fragmentation could counterintuitively promote disease outbreaks but that, for higher wildlife densities and longer infectious periods, small differences in how hosts navigated their environments could dramatically alter observed disease dynamics.

Author contributions: L.A.W., J.D.F., and M.E.C. designed research; L.A.W. performed research; L.A.W. and J.D.F. analyzed data; and L.A.W., J.D.F., and M.E.C. wrote the paper.

The authors declare no conflict of interest.

This article is a PNAS Direct Submission.

Data deposition: The code and simulation results reported in this paper are available at https://github.com/whit1951/landscape-sim.

[1]To whom correspondence should be addressed. Email: whit1951@umn.edu.

This article contains supporting information online at www.pnas.org/lookup/suppl/doi:10.1073/pnas.1801383115/-/DCSupplemental.

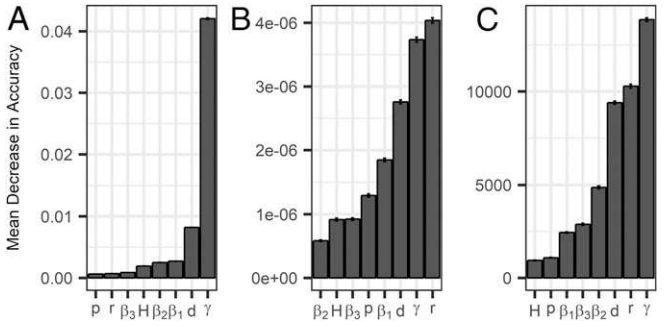

Fig. 1. Random forest regression analysis results describing variable importance for (*A*) outbreak success (did the pathogen spread beyond the initially infected individual?), (*B*) maximum prevalence given outbreak success, and (*C*) outbreak duration given outbreak success. Parameter descriptions are provided in Table 1. Bar charts display an unscaled mean decrease in accuracy for parameters; higher values for mean decrease in accuracy correspond to parameters with higher predictive ability. Error bars reflect SD of mean decrease in accuracy. The randomForest package in R (with 10,000 trees) was used for this analysis. While included in the random forest analysis, transmission rate (β) received a variable importance score of zero for all three metrics (as would be expected, since it did not vary in the factorial design) and is not depicted in Fig. 1.

question: how does individual movement behavior, governed by perceptual range and individual selection for resource availability and conspecific density, interact with spatial heterogeneity (via resource availability and clustering) to affect infectious disease dynamics? Specifically, we examined outbreak behavior through two questions: (*i*) Which epidemiological, movement, or landscape factors led to a successful outbreak (defined as spreading beyond the initially infected individual)? (*ii*) Given at least one secondary case, which factors best predicted maximum prevalence and duration? We developed an individual-based susceptible–infected–recovered (SIR) model for a theoretical host–pathogen system where an RSF governed host movement choices and pathogens were directly transmitted, assuming a density-dependent transmission function. We varied both landscape structure and movement parameters, and we quantified disease dynamics by the maximum prevalence and the duration of the outbreak. In addition, we compared our spatially explicit model output to a comparable SIR model that assumes homogeneous mixing. We propose a general theoretical framework to generate testable predictions for specific host–pathogen systems existing on complex landscapes.

Results

Which Factors Determine Whether an Outbreak Is Successful? The outbreak data are heavily skewed—most initial pathogen introductions never transmitted successfully to a second individual. Based on random forest analysis, recovery rate (γ) had the largest effect on whether there were any secondary cases beyond the initially infected individual (Fig. 1*A*). While conspecific density (d) was the next most influential parameter, it had less than one-fourth of the mean decrease in accuracy of recovery rate, suggesting that pathogen infectious period ($1/\gamma$) played an outsized role in determining whether an outbreak resulted in secondary cases (Fig. 1*A* and *SI Appendix*, Fig. S1*A*).

Given Secondary Cases, Which Parameters Most Influence Maximum Prevalence and Duration? If an outbreak spread successfully beyond the initially infected individual, the interaction of recovery rate, perceptual range, and conspecific density had strong effects on both maximum prevalence and duration for the simulations (Fig. 2). This finding was supported by the random forest analysis, which identified recovery rate, perceptual range, and conspecific density as the top three parameters in predictive value for both maximum prevalence and duration (Fig. 1 *B* and *C* and *SI Appendix*, Fig. S1 *B* and *C*). Overall, simulations with faster recovery rates ($\gamma = 0.4$), lower conspecific densities ($d = 0.25$), and smaller perceptual ranges ($r = 1, 2$) had fewer successful outbreaks, and outbreaks that were successful reached fewer individuals and were shorter in duration (Fig. 2 and *SI Appendix*, Fig. S2).

Beyond these top three influential parameters, the order of variable importance as identified by random forest analysis differed for maximum prevalence and duration. For maximum prevalence, selection for resources (β_1) and proportion of available habitat (p) outweighed strength of selection for conspecifics (β_2 and β_3) and degree of patchiness (H) (Fig. 1*B* and *SI Appendix*, Fig. S1*B*). In contrast, for mean duration, the strength of selection for conspecifics (β_2 and β_3) outweighed strength of selection for resources (β_1) and landscape structure (p and H) (Fig. 1*C* and *SI Appendix*, Fig. S1*C*).

Effects of Landscape Structure and Individual Movement Behavior. When holding the influential parameters of recovery rate, perceptual range, and conspecific density constant, interactions between landscape structure and individual movement behavior emerged. For simulations with lower conspecific density ($d = 0.25$) and faster recovery rates ($\gamma = 0.4$), epidemics were rarely successful (*SI Appendix*, Fig. S3 *E* and *F*). For simulations with lower conspecific density ($d = 0.25$) and slower recovery rates ($\gamma = 0.1$ and 0.2), more fragmented landscapes ($H \leq 0.5$) with lower resource availability ($p \leq 0.5$) exhibited larger outbreak size and lasted longer for more RSF combinations (*SI Appendix*, Fig. S3 *A–D*); this same pattern was observed for systems with both higher conspecific density ($d = 0.50$) and faster recovery rates ($\gamma = 0.2, 0.4$) (*SI Appendix*, Fig. S4 *C–F*). In general, positive selection for resources ($\beta_1 = 3, 6$) led to higher outbreak peaks and longer-lasting outbreaks compared with random selection for habitat ($\beta_1 = 0$) (Fig. 3 and *SI Appendix*, Fig. S5). However, for simulations with higher conspecific densities ($d = 0.5$), slower recovery rates ($\gamma = 0.1$), and higher perceptual ranges ($r = 3$), we observed more complex dynamics (Fig. 3 and *SI Appendix*, Figs. S4 *A* and *B* and S6) where RSFs interacted with landscape structure to determine epidemic dynamics (Fig. 4).

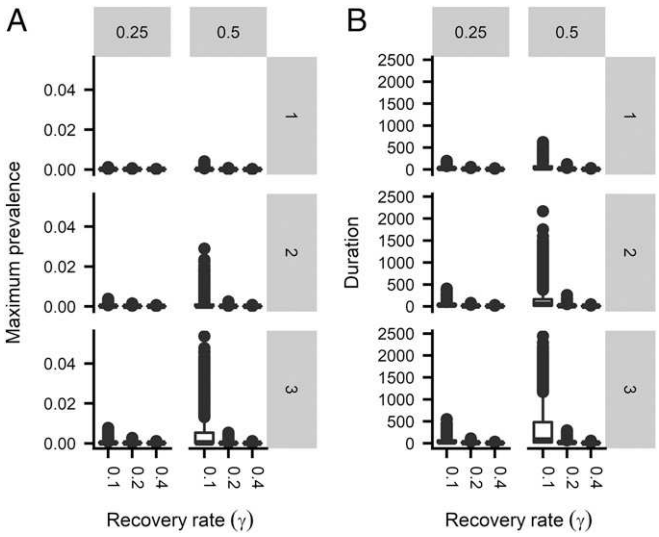

Fig. 2. Effects of recovery rate (x axis) on (*A*) maximum prevalence and (*B*) duration for successful outbreaks (number of secondary cases greater than or equal to one) across different conspecific densities (columns) and perceptual ranges (rows). These plots are combined for all RSFs and for all landscape structures. These outcomes for individual RSFs can be observed in *SI Appendix*, Fig. S2.

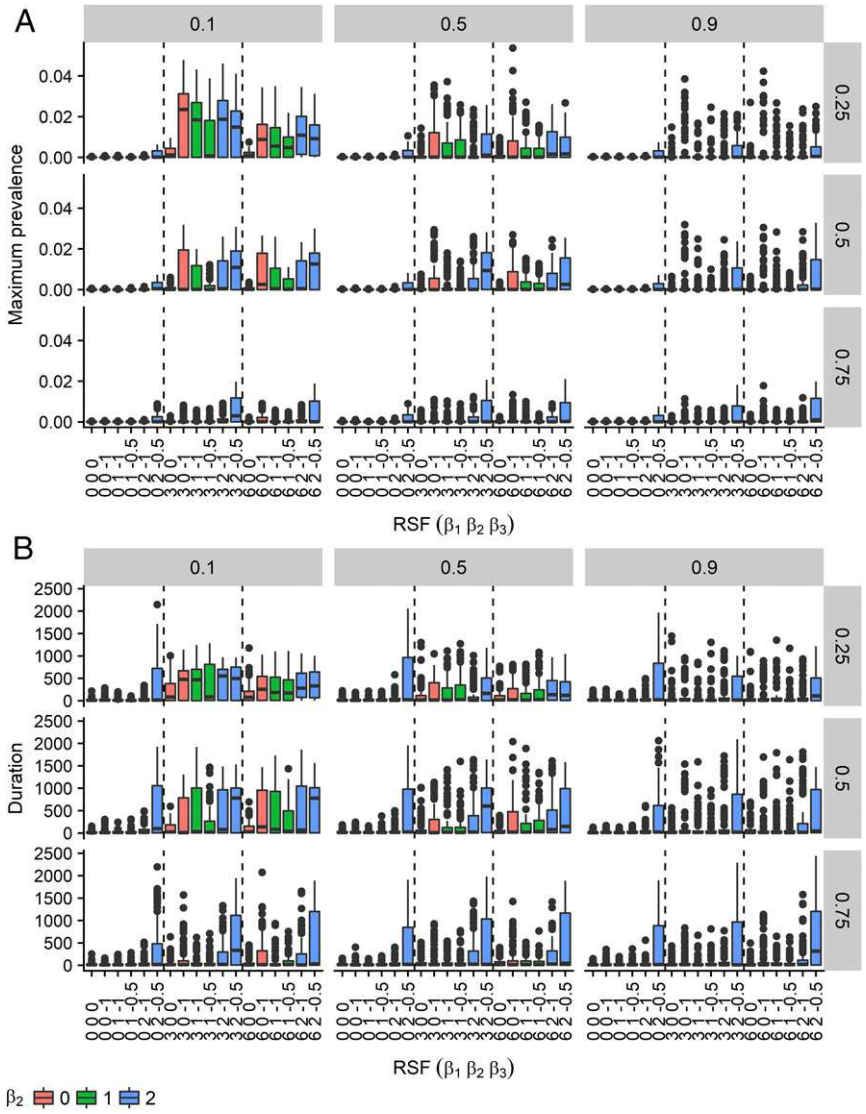

Fig. 3. Box plots of (*A*) maximum prevalence and (*B*) duration for a subset of the simulations where $\gamma = 0.1$, $d = 0.5$, and $r = 3$. Columns correspond to Hurst exponent (*H*; lower values correspond to higher clustering), and rows correspond to proportion available habitat (*p*). Dashed lines represent separate regimes of random, medium, or strong selection for resources (β_1).

For the parameter space exhibiting a higher proportion of successful outbreaks across RSFs ($r = 3$, $\gamma = 0.1$, $d = 0.5$), maximum prevalence was higher across more RSFs for more clustered habitat ($H = 0.1$) with lower resource availability ($p = 0.25$) (Fig. 3*A*). However, this did not necessarily correlate with duration. While outbreaks lasted longer on average for more RSFs in fragmented landscapes ($H = 0.1$ and $p = 0.25$), outbreaks lasted longer at intermediate clustering ($H = 0.5$) for certain RSFs (Figs. 3*B* and 4*B*). Overall, when hosts exhibited strong positive selection for both conspecifics ($\beta_1 = 3, 6$ and $\beta_2 = 1, 2$) and resources, disease outbreaks had the largest variation in duration for patchy landscapes ($H = 0.1$) with an intermediate proportion of available habitat ($p = 0.5$) (Fig. 3*B*). However, regardless of landscape structure, stronger selection for the presence of other conspecifics (e.g., $\beta_2 = 2$) reliably increased the observed duration of outbreaks (Fig. 3*B*). This threshold behavior for selection for conspecifics—where selection for conspecifics supersedes landscape structure—was not observed for landscapes with lower conspecific densities and faster recovery rates (*SI Appendix*, Figs. S3 and S5).

How Do These Results Compare with Models that Assume Homogenous Mixing? Compared with the spatially explicit movement model described here, the equivalent homogenous mixing model with density-dependent transmission consistently overestimated the maximum prevalence reached for both conspecific densities and all three simulated recovery rates (*SI Appendix*, Fig. S7*A*). In particular, for the higher perceptual range ($r = 3$), slowest recovery rate ($\gamma = 0.1$), and higher conspecific density treatment ($d = 0.5$), the homogeneous mixing model did not capture the skewed nature of observed epidemics' duration (*SI Appendix*, Fig. S7*B*).

Discussion

We were expecting landscape structure to have a substantial impact on simulated disease dynamics. While this was true to some extent, two of the top three covariates in variable importance as determined by random forest analysis (i.e., recovery rate and conspecific density) had nothing to do with landscape structure per se. However, perceptual range played a key role in determining maximum prevalence and duration of outbreaks (Fig. 1 *B* and *C*), and perceptual range functionally defines the landscape that an individual host perceives. Other modeling studies have

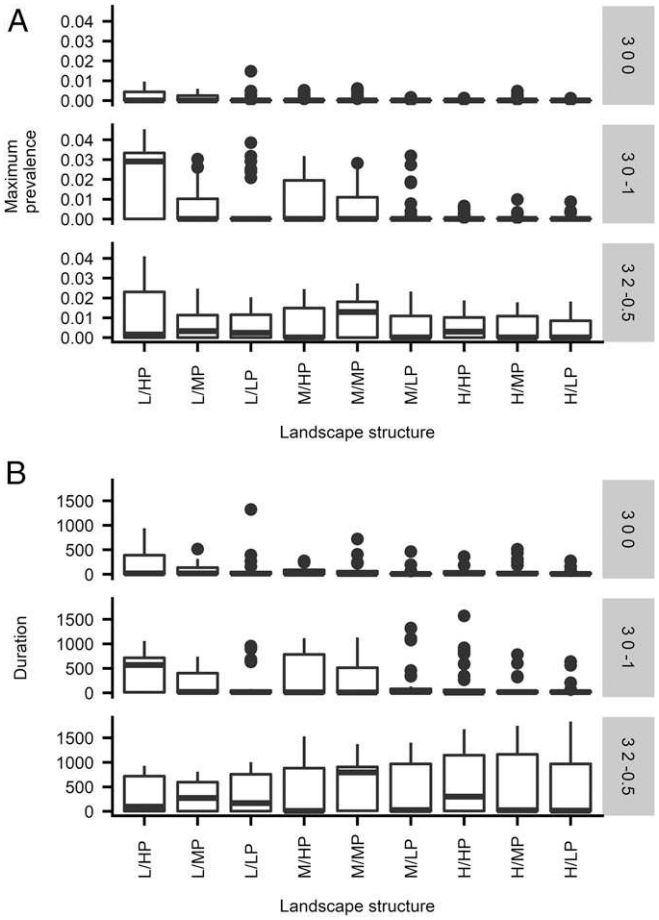

Fig. 4. Box plots of (*A*) maximum prevalence and (*B*) duration for three RSFs when recovery rate (γ) = 0.1, conspecific density (d) = 0.5, and perceptual range (r) = 3. The RSFs (rows: β_1 β_2 β_3) correspond to three biological scenarios: (*i*) positive selection for resources ($\beta_1 = 3$, $\beta_2 = 0$, $\beta_3 = 0$), (*ii*) positive selection for resources with conspecific avoidance ($\beta_1 = 3$, $\beta_2 = 0$, $\beta_3 = -1$), and (*iii*) positive selection for resources with conspecific attraction ($\beta_1 = 3$, $\beta_2 = 2$, $\beta_3 = -0.5$) (*SI Appendix*, Fig. S8). Landscape structure abbreviations take the form of proportion available habitat (*p*)/patchiness (Hurst exponent, *H*): H, high proportion available habitat; HP, high patchiness; L, low; LP, low patchiness; M, medium; MP, medium patchiness.

verified the potential importance of perceptual range in determining landscape connectivity (16), and our results emphasize the concomitant implications for pathogen spread and persistence. This suggests that the incorporation of plastic perceptual ranges may also be important for future disease models (17).

When holding these top three influential parameters (recovery rate, conspecific density, and perceptual range) constant, fragmentation promoted pathogen outbreaks and persistence for most of the explored parameter space, particularly for simulations with combinations of (*i*) lower conspecific densities and slower recovery rates (*SI Appendix*, Fig. S3 *A–D*) or (*ii*) higher conspecific densities and faster recovery rates (*SI Appendix*, Fig. S4 *C–F*). However, this pattern was highly dependent on hosts being able to perceive more of their habitat to be able to make movement decisions (e.g., a larger perceptual range) (*SI Appendix*, Figs. S3 and S4). Positive selection for resources was also necessary to elicit differences in pathogen spread in response to landscape structure, particularly at faster recover rates (Fig. 3 and *SI Appendix*, Fig. S5). In an applied setting, these results highlight the potential role of resource hotspots and resource provisioning in altering not only animal movement patterns but also, subsequent pathogen transmission (18). Resource hotspots can occur naturally (e.g., carcasses acting as landscape hotspots for transmission of rabies in jackals) (19) or artificially through human supplementation [e.g., *Mycoplasma gallisepticum* transmission at bird feeders (20) or brucellosis transmission from supplemental feeding of elk in Yellowstone National Park (21)]. While such selection could apply to foraging choices, it could also apply to selection for burrows or dens. For example, in desert tortoises (*Gopherus agassizii*), contacts primarily occurring in underground burrows are thought to drive transmission of *Mycoplasma agassizii* (22).

At higher perceptual range ($r = 3$), slower recovery rates ($\gamma = 0.1$), and higher conspecific densities ($d = 0.5$), we captured more nuanced and complex behavior that resulted from interactions between landscape structure, movement behavior, and recovery rate (Figs. 3 and 4). Notably, a comparable homogenous-mixing, density-dependent SIR model did not capture the skewed distribution of epidemic duration found for simulations in this parameter space (*SI Appendix*, Fig. S7*B*). Outbreaks reaching the most individuals generally occurred in more fragmented landscapes ($H = 0.1, p = 0.1$) (Fig. 3*A*), but outbreaks in patchy/medium proportion habitat landscapes ($H = 0.1, p = 0.5$) lasted longer for some RSFs and exhibited more variation in observed duration (Figs. 3*B* and 4*B* and *SI Appendix*, Fig. S6*F*). Also, threshold behavior was exhibited for selection for conspecifics in this parameter space; very strong selection for conspecifics ($\beta_2 = 2$) promoted longer-lasting outbreaks with higher maximum prevalence regardless of landscape structure (Fig. 3). This was interesting, because relatively small differences in RSF values resulted in substantially different disease dynamics (*SI Appendix*, Fig. S8). For such regimes, we suggest that it may be important to model individual responses to landscape structure to better capture the dynamics of a given disease.

The model presented here best describes direct transmission of a single infectious agent (or limited indirect transmission as defined by aerosolized transmission or limited fomite persistence relative to movement time steps) within a single host species experiencing density-dependent transmission. Thus, these results are applicable to host–pathogen systems that have previously been favored in a spatial modeling context, including rabies and bTB (2, 12). For example, a recent model of raccoon rabies found that inadequate levels of vaccination in continuous, poor-quality habitat could prove counterproductive, leading to outbreaks (4). Our findings are also relevant to emerging pathogens ranging from Ebola or respiratory viruses among primate species to bat-to-bat transmission of Hendra virus (23, 24). For example, a recent spatially structured model for Hendra virus in fruit bats found that habitat loss led to congregation in urban roosting sites and reduced migration, which could aid in disease persistence and in spillover to humans (24). Since conspecific density played a key role in determining the relationship between outbreak success and fragmentation, this work might be particularly relevant to wildlife populations where host densities vary widely through time [e.g., Moepia virus or Hantavirus in rodents, where direct transmission via agonistic interactions is known to be important (25, 26)].

We recognize that many host–pathogen systems experience more complex transmission cycles than represented by this model; we would expect dynamics to differ with the incorporation of demographic processes (births and deaths), disease-related mortality from a more lethal pathogen (e.g., rabies), a substantial incubation period, or chronic infection (e.g., bTB). While this work does not explicitly address the potential effects of pathogen coinfection (27), multihost pathogens [e.g., canine distemper virus (28)], indirect transmission or environmental persistence [e.g., chronic wasting disease (29)], or vector foraging behavior [e.g., Lyme disease (30)], the results of this research could easily be extended to more biologically complex systems.

Future studies could build in additional landscape complexity or focus on more realistic mechanisms governing movement

choices. For instance, we modeled pathogen transmission across theoretical binary landscapes. Realistically, movement choices are influenced by a variety of landscape covariates, not just presence or absence of resources (31). Similarly, we considered each cell in the landscape to be equally permeable—other than relative distance from the host, there was no cost to traversing bad-quality habitat relative to good-quality habitat. In addition, we did not model depletion of resources explicitly but rather, through reaction of individuals to other conspecifics (β_2 and β_3). This helped us limit the number of assumptions built into the model, but it certainly simplifies the proximate mechanisms of foraging behavior (32). Finally, for a given simulation, all individuals responded the same way to the presence of resources and conspecifics. We note that, for many systems, there will be individual variability in foraging and social behavior, and these differences may merit further consideration for some host–pathogen systems (33). For instance, a recent study of raccoons and contact risk for rabies determined that a subset of individuals was responsible for the majority of risky contacts, despite all individuals following the same movement rules (34). Finally, we ignored the fact that animal movement behavior can change with infection (8).

A recent systematic review investigating the relationship between pathogen transmission and anthropogenic land use change found that a majority of studies linked anthropogenic change with higher transmission risk (35). Overall, our work has important implications for how pathogens spread across fragmented and human-influenced landscapes and supports other modeling studies that have suggested that fragmentation can have nonlinear effects on pathogen persistence in specific host–pathogens systems (4, 5, 36) and that spatial hotspots of transmission can emerge from limited high-quality resource sites (36–38). This work provides a theoretical mechanistic framework that can be expanded to specific host–pathogen systems to provide testable hypotheses about the influence of landscape structure and movement behavior on disease dynamics, thus providing a critical bridge between the disciplines of movement and disease ecology (2, 11, 12). We hope that this model inspires additional consideration of how landscape structure may influence disease dynamics and foster investigation of these questions in specific host–pathogen systems and applied management settings.

Methods

We developed a stochastic, individual-based SIR model for a nonlethal pathogen in a closed population (i.e., no births, deaths, immigration, or emigration). Individuals could move across a spatially explicit, discrete lattice landscape, where resource presence or absence was variable in space (*SI Appendix*, Fig. S9). Using the midpoint displacement algorithm, we generated theoretical binary neutral landscapes that varied in the proportion of available habitat (***p***) and the degree of habitat clumping (Hurst exponent, ***H***) (39). We assumed a torus shape (i.e., wrapped boundaries) for these landscapes to avoid edge effects (40).

An RSF and a 2D movement kernel modulated individual movement choices across these theoretical landscapes. For a habitat of $\boldsymbol{k} = 1, \ldots, \boldsymbol{m}$ discrete grid cells, the probability of an individual moving from current location, ***a***, to new location, ***b***, over a fixed temporal time step is $\mathrm{P}(\boldsymbol{a}\text{ to }\boldsymbol{b}) = \phi(\boldsymbol{a},\boldsymbol{b})\boldsymbol{w_b}/\sum_{\boldsymbol{k}=1}^{\boldsymbol{m}}[\phi(\boldsymbol{a},\boldsymbol{c_k})\boldsymbol{w_k}]$, where $\phi(\cdot)$ is a 2D movement kernel in the absence of habitat selection, $\boldsymbol{c_k}$ represents the center point of each grid cell, and $\boldsymbol{w_b}$ and $\boldsymbol{w_k}$ are RSFs governing an individual's movement preferences for cells ***b*** and ***k***, respectively. Generally, an RSF for any given cell ***j*** takes the form $\boldsymbol{w_j} = \exp(\beta_1 \cdot \boldsymbol{R_j} + \beta_2 \cdot \boldsymbol{N_j} + \beta_3 \cdot \boldsymbol{N_j^2})$. The parameters $\boldsymbol{R_j}$ and $\boldsymbol{N_j}$ correspond to the resource quality and number of conspecifics, respectively, in cell ***j***. The coefficients $\beta_1, \beta_2,$ and β_3 govern the strength of selection that resource quality and the number of conspecifics play in habitat choice (31). In particular, because conspecific density changes through time across a static resource landscape, the inclusion of the quadratic term β_3 allows us to test three biologically feasible scenarios in response to the presence of conspecifics: (*i*) individuals avoid conspecifics, (*ii*) individuals are attracted to conspecifics (signaling good-quality habitat) until there are tradeoffs with resource depletion, and (*iii*) individuals make movement choices irrespective of conspecifics (more on how we calibrated values for the RSF is in *SI Appendix*). We began by assuming a Moore neighborhood (eight neighboring cells) but subsequently tested the effects of larger continuous perception and relocation kernels (Table 1). We assumed the simplest case, where the movement kernel is inversely proportional to radial distance from the center point of the current grid cell and acts in the absence of resource availability: $\phi(\boldsymbol{r}) = 1/2\pi\boldsymbol{r}^2$, where $r = \sqrt{(x_a - x_{c_k})^2 + (y_a - y_{c_k})^2}$.

The equation gives an inverse distance weight (i.e., $1/r$) that is multiplied by the circumference at that distance to account for a uniform circular distribution (i.e., $1/2\pi r$).

We conducted 100 replications per parameter set, and we used a factorial design to explore the relative effects of recovery rate, conspecific density, landscape structure, RSFs, and perceptual range on disease dynamics (Table 1 and *SI Appendix*, Fig. S9). We calibrated the transmission probability (β) to be able to test reasonable values of the basic reproductive rate R_0(for an SIR model, $R_0 \sim \beta/\gamma$). Under that framework, we tested values of $R_0 \sim 0.5, 1,$ and 2 in our simulations (Table 1 and *SI Appendix, SI Text*).

Each simulation began with a single infectious individual and continued until there were no remaining infectious individuals on the landscape. At each time step, every individual in the simulation had the opportunity to evaluate the surrounding environment and move to a cell within the perceptual range. After all individuals had been given the opportunity to relocate, the possibility of transmission was evaluated; we assumed that transmission could occur only between individuals of the same cell during the same time step. The probability of a susceptible individual becoming infected was represented by $\mathrm{P}(T) = 1 - (1-\beta)^I$, where β is the transmission rate and I is the number of infectious individuals in the same cell. After potential transmission events, infected individuals could also recover with a probability, γ, at each time step. This corresponded to an average infectious period of the pathogen of $1/\gamma$ (Table 1).

We compared the spatially explicit model results with a simpler stochastic SIR model that assumes density-dependent transmission and homogeneous mixing. This was simulated with a Reed Frost model, in which cumulative probability of transmission during at time step, τ, is equal to $\mathrm{P}_\tau = 1 - (1-\beta)^{I_\tau}$,

Table 1. Factorial design of 2,916 parameter combinations encompassing epidemiology, movement behavior, and landscape structure

Parameter	Levels	Values
Conspecific density (*d*; individuals per unit area of simulated landscape)	Low, medium	0.25, 0.5
Transmission rate (β)	Constant	0.2
Recovery rate (γ); conversely, infectious period ($1/\gamma$)	Slow, medium, fast; long, medium, short infectious periods	0.1, 0.2, 0.4 time^{-1}; 10, 5, 2.5 time steps
Proportion of available habitat (p)	Low, medium, high	0.25, 0.50, 0.75
Clustering of habitat (H)	Low, medium, high	0.1, 0.5, 0.9
Strength of selection for resources (β_1)	None (random), low, high	0, 3, 6
Strength of selection for conspecifics (β_2, β_3)	None (random), avoidance, attraction	(0, 0), (0, −1), (1, −1), (1, −0.5), (2, −1), (2, −0.5)
Perceptual range (r)	Low, medium, high	1, 2, 3

We conducted 100 simulations per parameter set. More information on how the RSF parameters ($\beta_1, \beta_2, \beta_3$) were calibrated and how these values correspond to movement choices is in *SI Appendix, SI Text*.

where β equals the per contact transmission risk and I_τ equals the number of infectious individuals at time step τ. The number of infected individuals at the next time step is then given by $I_\tau = \text{Binomial}(S_\tau, P_\tau)$. Unlike for the spatially explicit simulations, this probability was evaluated for the entire population, not just a single cell in the landscape. The results from this simple stochastic simulation were verified with the output from comparable deterministic ordinary differential equations (*SI Appendix, SI Text*).

Finally, we used random forest analysis—a machine learning method—to tease apart the relative contributions of parameters to outbreak outcomes. As a recursive partitioning method, random forest analysis fits a single predictive model by synthesizing the predictions from numerous classification or regression trees (41, 42). The random forest approach has several advantages for ecological data; most notably, this approach can handle complicated, nonlinear, and potentially collinear relationships between predictor variables (41, 42). This approach also avoids some of the pitfalls of using a frequentist approach to analyze simulation results, since sample size in simulation studies is arbitrary and can result in significant *P* values regardless of effect size (43). Other disease model studies have used this approach to better understand complex data with multiple predictors (44, 45).

Variable importance measures from random forest analysis describe the relative role that a covariate plays in deciding model outcomes (42). We used the randomForest package in R (46) to calculate variable importance scores so that we could understand what factors affected three separate response variables: (*i*) outbreak success (did the pathogen spread beyond the initially infected individual?); given successful transmission, (*ii*) maximum prevalence and (*iii*) duration of the outbreak. For covariates, we included conspecific density, transmission rate, recovery rate, landscape structure (*p* and *H*), individual movement preferences (as governed by the RSF: $\beta_1, \beta_2, \beta_3$), and perceptual range (Table 1). We report variable importance scores in terms of mean decrease in accuracy, which is equivalent to percentage increase in mean square error for regression random forest analyses (46). Mean decrease in accuracy corresponds to the loss of predictive value for the model when a parameter is permutated randomly rather than using its given value (42). We report raw variable importance measures that have not been scaled by the SE, as these values may be less biased for correlated predictors (47). We also corroborated variable importance results by conducting a secondary analysis using the cforest function from the party package in R (47). This approach has been shown to have a more robust estimate of variable importance (47); however, this comes with a computational cost. After reducing our analysis to 1,000 trees (so that computational time was tractable in cforest), we found that our main conclusions were still supported, with the only changes being the order of lower-ranked variables with very similar importance values (*SI Appendix*, Fig. S1). All simulations and analyses were conducted in R (version 3.3.2). Code and simulation results are available at https://github.com/whit1951/landscape-sim.

ACKNOWLEDGMENTS. We acknowledge the Minnesota Supercomputing Institute at the University of Minnesota for providing resources that contributed to the research results reported within this paper (https://www.msi.umn.edu/). L.A.W. was funded by National Science Foundation Grants GRFP-00039202 and DEB-1701069 and the University of Minnesota Informatics Institute. M.E.C. was funded by National Science Foundation Grants DEB-1413925 and DEB-1654609, the University of Minnesota's Office of the Vice President for Research and Academic Health Center Seed Grant.

1. Keeling M, Rohani P (2008) *Modeling Infectious Diseases in Humans and Animals* (Princeton Univ Press, Princeton).
2. White LA, Forester JD, Craft ME (2018) Dynamic, spatial models of parasite transmission in wildlife: Their structure, applications and remaining challenges. *J Anim Ecol* 87:559–580.
3. Hagenaars TJ, Donnelly CA, Ferguson NM (2004) Spatial heterogeneity and the persistence of infectious diseases. *J Theor Biol* 229:349–359.
4. Rees EE, Pond BA, Tinline RR, Bélanger D (2013) Modelling the effect of landscape heterogeneity on the efficacy of vaccination for wildlife infectious disease control. *J Appl Ecol* 50:881–891.
5. Tracey JA, Bevins SN, Vandewoude S, Crooks KR (2014) An agent-based movement model to assess the impact of landscape fragmentation on disease transmission. *Ecosphere* 5:art119.
6. Lloyd-Smith JO (2010) Modeling density dependence in heterogeneous landscapes: Dispersal as a case study. *J Theor Biol* 265:160–166.
7. Brown LM, Crone EE (2016) Individual variation changes dispersal distance and area requirements of a checkerspot butterfly. *Ecology* 97:106–115.
8. Welicky RL, Sikkel PC (2015) Decreased movement related to parasite infection in a diel migratory coral reef fish. *Behav Ecol Sociobiol* 69:1437–1446.
9. Lima SL, Zollner PA (1996) Towards a behavioral ecology of ecological landscapes. *Trends Ecol Evol* 11:131–135.
10. Lane-deGraaf KE, et al. (2013) A test of agent-based models as a tool for predicting patterns of pathogen transmission in complex landscapes. *BMC Ecol* 13:35.
11. Fofana AM, Hurford A (2017) Mechanistic movement models to understand epidemic spread. *Philos Trans R Soc Lond B Biol Sci* 372:20160086.
12. Dougherty ER, Seidel DP, Carlson CJ, Spiegel O, Getz WM (2018) Going through the motions: Incorporating movement analyses into disease research. *Ecol Lett* 21:588–604.
13. Campomizzi AJ, et al. (2008) Conspecific attraction is a missing component in wildlife habitat modeling. *J Wildl Manage* 72:331–336.
14. Oliveira-Santos LGR, Forester JD, Piovezan U, Tomas WM, Fernandez FAS (2016) Incorporating animal spatial memory in step selection functions. *J Anim Ecol* 85:516–524.
15. Smouse PE, et al. (2010) Stochastic modelling of animal movement. *Philos Trans R Soc Lond B Biol Sci* 365:2201–2211.
16. Pe'er G, Kramer-Schadt S (2008) Incorporating the perceptual range of animals into connectivity models. *Ecol Modell* 213:73–85.
17. Olden JD, Schooley RL, Monroe JB, Poff NL (2004) Context-dependent perceptual ranges and their relevance to animal movements in landscapes. *J Anim Ecol* 73:1190–1194.
18. Becker DJ, Hall RJ (2016) Heterogeneity in patch quality buffers metapopulations from pathogen impacts. *Theor Ecol* 9:197–205.
19. Borchering RK, Bellan SE, Flynn JM, Pulliam JRC, McKinley SA (2017) Resource-driven encounters among consumers and implications for the spread of infectious disease. *J R Soc Interface* 14:20170555.
20. Dhondt AA, Dhondt KV, Hawley DM, Jennelle CS (2007) Experimental evidence for transmission of *Mycoplasma gallisepticum* in house finches by fomites. *Avian Pathol* 36:205–208.
21. Cross PC, Edwards WH, Scurlock BM, Maichak EJ, Rogerson JD (2007) Effects of management and climate on elk brucellosis in the Greater Yellowstone Ecosystem. *Ecol Appl* 17:957–964.
22. Aiello CM, et al. (2016) Host contact and shedding patterns clarify variation in pathogen exposure and transmission in threatened tortoise Gopherus agassizii: Implications for disease modelling and management. *J Anim Ecol* 85:829–842.
23. Rushmore J, et al. (2013) Social network analysis of wild chimpanzees provides insights for predicting infectious disease risk. *J Anim Ecol* 82:976–986.
24. Plowright RK, et al. (2011) Urban habituation, ecological connectivity and epidemic dampening: The emergence of Hendra virus from flying foxes (Pteropus spp.). *Proc Biol Sci* 278:3703–3712.
25. Goyens J, Reijniers J, Borremans B, Leirs H (2013) Density thresholds for Mopeia virus invasion and persistence in its host *Mastomys natalensis*. *J Theor Biol* 317:55–61.
26. Clay CA, Lehmer EM, Previtali A, St Jeor S, Dearing MD (2009) Contact heterogeneity in deer mice: Implications for Sin Nombre virus transmission. *Proc Biol Sci* 276:1305–1312.
27. Knowles SCL, et al. (2013) Stability of within-host-parasite communities in a wild mammal system. *Proc Biol Sci* 280:20130598.
28. Craft ME, Hawthorne PL, Packer C, Dobson AP (2008) Dynamics of a multihost pathogen in a carnivore community. *J Anim Ecol* 77:1257–1264.
29. Almberg ES, Cross PC, Johnson CJ, Heisey DM, Richards BJ (2011) Modeling routes of chronic wasting disease transmission: Environmental prion persistence promotes deer population decline and extinction. *PLoS One* 6:e19896.
30. Li S, Gilbert L, Harrison PA, Rounsevell MDA (2016) Modelling the seasonality of Lyme disease risk and the potential impacts of a warming climate within the heterogeneous landscapes of Scotland. *J R Soc Interface* 13:20160140.
31. Forester JD, Im HK, Rathouz PJ (2009) Accounting for animal movement in estimation of resource selection functions: Sampling and data analysis. *Ecology* 90:3554–3565.
32. Rands SA, Pettifor RA, Rowcliffe JM, Cowlishaw G (2004) State-dependent foraging rules for social animals in selfish herds. *Proc Biol Sci* 271:2613–2620.
33. Klein S, Pasquaretta C, Barron AB, Devaud J-M, Lihoreau M (2017) Inter-individual variability in the foraging behaviour of traplining bumblebees. *Sci Rep* 7:4561.
34. Tardy O, Massé A, Pelletier F, Fortin D (2018) Interplay between contact risk, conspecific density, and landscape connectivity: An individual-based modeling framework. *Ecol Modell* 373:25–38.
35. Gottdenker NL, Streicker DG, Faust CL, Carroll CR (2014) Anthropogenic land use change and infectious diseases: A review of the evidence. *EcoHealth* 11:619–632.
36. Bonnell TR, Sengupta RR, Chapman CA, Goldberg TL (2010) An agent-based model of red colobus resources and disease dynamics implicates key resource sites as hot spots of disease transmission. *Ecol Modell* 221:2491–2500.
37. Benavides J, Walsh PD, Meyers LA, Raymond M, Caillaud D (2012) Transmission of infectious diseases en route to habitat hotspots. *PLoS One* 7:e31290.
38. Nunn CL, Thrall PH, Kappeler PM (2014) Shared resources and disease dynamics in spatially structured populations. *Ecol Modell* 272:198–207.
39. Turner MG, Gardner RH, O'Neill R (2001) *Landscape Ecology in Theory and Practice: Pattern and Processs* (Springer, New York), 2nd Ed.
40. With KA (1997) The application of neutral landscape models in conservation biology. *Conserv Biol* 11:1069–1080.
41. Breiman L (2001) Random forests. *Mach Learn* 45:5–32.
42. Cutler DR, et al. (2007) Random forests for classification in ecology. *Ecology* 88:2783–2792.
43. White JW, Rassweiler A, Samhouri JF, Stier AC, White C (2014) Ecologists should not use statistical significance tests to interpret simulation model results. *Oikos* 123:385–388.
44. Herrick KA, Huettmann F, Lindgren MA (2013) A global model of avian influenza prediction in wild birds: The importance of northern regions. *Vet Res (Faisalabad)* 44:42.
45. Kane MJ, Price N, Scotch M, Rabinowitz P (2014) Comparison of ARIMA and random forest time series models for prediction of avian influenza H5N1 outbreaks. *BMC Bioinformatics* 15:276.
46. Liaw A, Wiener M (2002) Classification and regression by randomForest. *R News* 2:18–22.
47. Strobl C, Hothorn T, Zeileis A (2009) Party on! A new, conditional variable-importance measure for random forests available in the party package. *R J* 1:14–17.